COOKOFF OF A MELT-CASTABLE EXPLOSIVE (COMP-B)

M.L. Hobbs, M. J. Kaneshige, and M. U. Anderson
Sandia National Laboratories†
Albuquerque, NM

ABSTRACT

A model for cookoff of Composition B (Comp-B) was developed using data from multiple sources. Comp-B is a mixture of 60 wt% RDX (hexahydro-1,3,5-trinitro-s-triazine) and 40 wt% TNT (2,4,6-trinitrotoluene) with or without a wax desensitizer. The single-phase reactive flow model assumes that the Comp-B, gas products, and condensed products move at the same velocity and are at the same temperature. Thus, three species continuity equations, a single energy equation, and a single laminar flow equation were solved for the three-dimensional distribution of temperature, velocity, and species. For these low Mach number flows, the pressure is only a function of time, i.e. P (x,y,z,t) = P(t). A simplified one-step, first-order, pressure-dependent reaction mechanism was used as a source in the species and energy equations. A hydrostatic Boussinesq source (ρg) was used for the momentum equation to determine the buoyancy driven flow. Both open (constant pressure) and closed (dynamic pressure) systems were evaluated. Differential Scanning Calorimeter (DSC) data indicate that the TNT component in Comp-B melts at the same temperature as pure TNT. However, the RDX seems to dissolve in the hot TNT showing a slight endothermic reaction at temperatures well below the melting point of RDX. Results support the hypothesis that ignition time and ignition location during cookoff of Comp-B are strongly dependent on reactive flow.

INTRODUCTION

Composition B (Comp-B) explosives consist of mixtures of RDX (1,3,5-Trinitro-1,3,5-triazacyclohexane), TNT (2,4,6-Trinitrotoluene), and a desensitizing wax. In the current work, Comp-B is assumed to be composed of 60/40 RDX/TNT by weight. Comp-B was developed prior to WWI by the Germans and the British, and has been used in mortar shells, torpedoes, demolition charges, warheads, shaped charges, and large bombs [1]. Comp-B is prepared by melting TNT in a steam-jacketed kettle, adding wet RDX slowly, heating and stirring until the water is evaporated. The Comp-B is then cast into the desired shape and cooled. Comp-B is easy to process, and has a high detonation pressure, but fails many insensitive munitions (IM) requirements [2]. Currently, IMX-104 is being evaluated as a replacement for Comp-B [3].

Comp-B does not pass slow and fast cookoff IM tests [2]. Consequently, the response of Comp-B during an accident, such as a fire, is important for safety analysis. The response is complicated by many factors such as melting of TNT, dissolution of RDX in hot liquid TNT, pressure-dependent kinetics, buoyancy driven convective flow, forced convection caused by decomposition gas bubbles, non-Newtonian viscosity, volumetric expansion, thermal conductivity, specific heat, and decomposition product composition at elevated temperature and pressure.

Most modeling of runaway ignition behavior in Comp-B has focused on thermal-chemistry effects with little regard to mechanical behavior such as pressurization and flow. For example, Zerkle presented a decomposition model of Comp-B [4] by combining a TNT and RDX

† Sandia National Laboratories is a multi-program laboratory managed and operated by Sandia Corporation, a wholly owned subsidiary of Lockheed Martin Corporation, for the U.S. Department of Energy's National Nuclear Security Administration under contract DE-AC04-94AL85000. SAND NO. 2012-XXXX.

decomposition mechanisms. The TNT model was based on McGuire and Tarver's TNT decomposition mechanism [5], and the RDX decomposition model was based on the work of Maharrey and Behrens [6]. Each of the separate TNT and RDX decomposition models were fit to match the ODTX data. However, when these models were combined using simple mixture rules, the predicted ignition times for Comp-B were much higher than the measured ignition times. Zerkle suggested the dissolution of RDX into molten TNT effectively reduces the activation barrier, causing the mixture to ignite sooner.

The TNT in Comp-B melts ~81°C, which is the same melting point as pure TNT. When all of the TNT is melted, the RDX remains suspended in the liquid TNT. As the temperature increases, the RDX dissolves in the hot TNT, between 127°C and 187°C. This is lower than the melting point of RDX, 205°C. There is little movement in the suspension until most of the RDX is dissolved. As temperature increases, the liquid decomposes into gases that form bubbles causing forced convection. Eventually, the reaction energy is generated faster that can be dissipated by convection and conduction leading to runaway ignition of the hot liquid.

Decomposition of RDX and TNT decomposition have previously been modeled using a single-step, first-order, pressure-dependent reaction with a normally distributed activation energy [7,8]. In the current work, the same kinetic form as described in [7,8] was used to model Comp-B, and a hydrostatic Boussinesq source (ρg) was used with the momentum equation to determine the buoyancy driven flow, similar to that used in [7]. However, in [7], the melting front of TNT was not determined. In the current work, the melting front is calculated using a temperature dependent viscosity that is high for the solid and low for the liquid. Kinetic parameters were obtained from data in Sandia's instrumented thermal ignition experiment (SITI) and the model is validated using a larger cookoff test performed in a convective oven.

EXPERIMENTAL OBSERVATIONS

TGA/DTA/DSC

Figure 1 shows data from thermogravimetric analysis (TGA) and differential thermal analysis (DTA) for RDX, TNT, and Comp-B from [9]. The TGA data, which shows mass loss with increasing temperature, are for nominally 10 mg samples heated at ~10°C/min in a nitrogen atmosphere. The onset of mass loss for the RDX, TNT, and Comp-B samples occurs at 226°C, 190°C, and 145°C, respectively. The early onset of Comp-B decomposition may be attributed to the hot liquid TNT dissolving the RDX suspension. RDX reacts faster in the liquid phase than in the solid phase as discussed by Brill et al. [10].

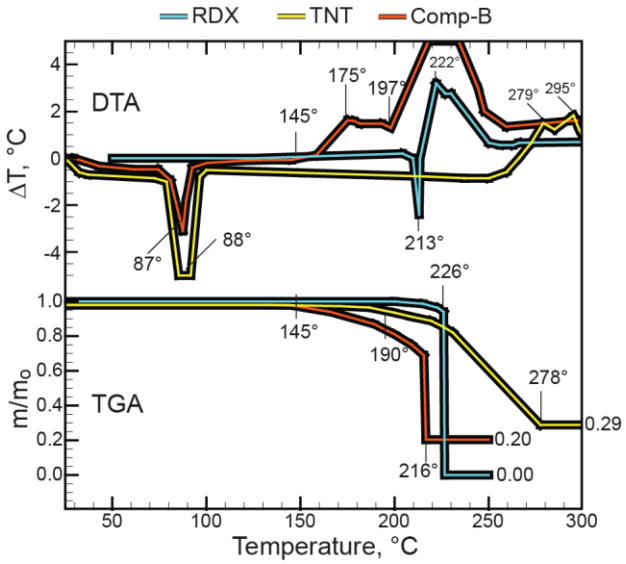

Fig. 1. DTA and TGA for RDX, TNT, and Comp-B (data interpolated from

The DTA results in Figure 1 show that the TNT in Comp-B melts at the same temperature as in pure TNT. The melting of TNT is an endothermic phase change that occurs at temperatures that are lower than reaction thresholds that initiate mass loss. In contrast, the RDX melting point is absent in the Comp-B DTA data. The Comp-B DTA curve shows the onset of an exothermic reaction at 145°C, which is quenched at 175°C by an apparent endothermic reaction that may be related to the dissolution of the RDX suspension.

The trends shown in Figure 1 are not quantitative. For example, the DTA for TNT shows an exotherm in the TNT data peaking between 279°C and 295°C. However, the TGA data for TNT shows no reaction after 278°C. The TNT and RDX samples in Figure 1 were probably not the same TNT and RDX used to make the Comp-B samples in Figure 1. Furthermore, the TGA mass loss was measured in a separate experiment and may not correspond to the DTA data in Figure 1. Combined TGA and differential scanning calorimetry (DSC) better quantify the thermal stability of Comp-B as shown in Figure 2.

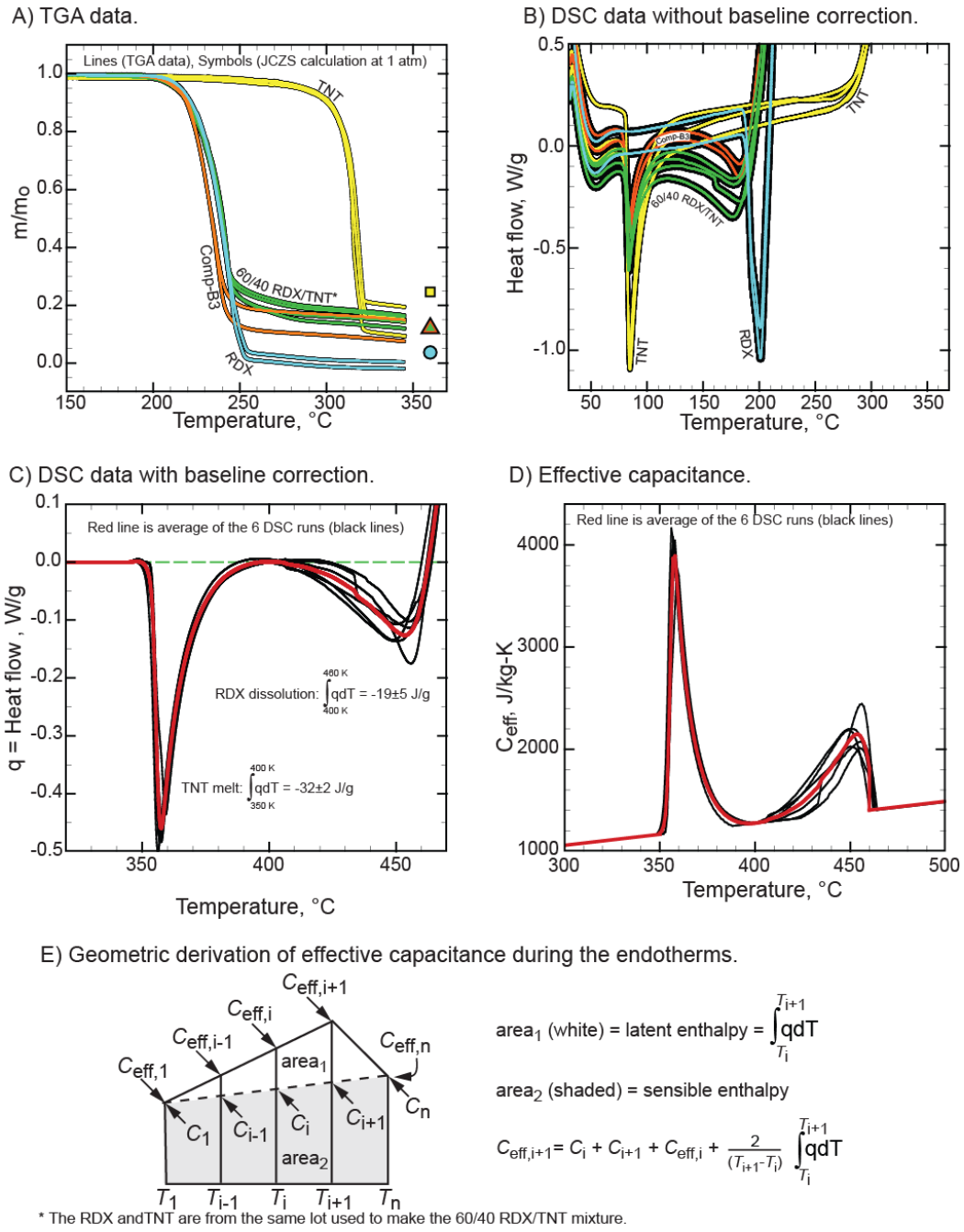

Fig. 2. Simultaneous TGA/DSC data showing effective capacitance model.

Figures 2.A and 2.B show simultaneous TGA/DSC data for TNT, RDX, and Comp-B with the 4.68±0.31 mg samples ramped at 10°C/min. A custom 60/40 mixture of TNT and RDX was made and is labeled 60/40 RDX/TNT in Figures 2.B and 2.B. The custom 60/40 mixture was made with the same lot of material that was used for the individual TNT and RDX TGA/DSC runs. There were four TNT runs (two with common TNT flakes and two from pure four times recrystallized TNT), two RDX runs (type II, class 1 RDX), two Comp-B runs (Comp-B3 which does not contain wax), and four custom 60/40 RDX/TNT runs. The RDX in the custom 60/40 RDX/TNT mixture was type II class 1 RDX. Two of the custom 60/40 RDX/TNT mixtures used common TNT flakes and the other two custom mixtures used the pure TNT. The symbols in Figure 4.A are the remaining solid fraction calculated with the JCZS-EOS [11] at 360°C for TNT (yellow square), Comp-B (orange triangle), the custom 60/40 RDX/TNT mixture (small green triangle in the middle of the orange triangle), and the RDX (cyan circle).

Figure 2.C shows the six baseline corrected DSC runs (2 of the Comp-B3 runs and 4 of the custom 60/40 RDX/TNT runs). The average of the six runs is also shown as a red line in Figure 2.C. The integral of the average heat flow between 77°C (350 K) and 127°C (400 K) is the latent enthalpy required to melt the TNT (-32 $J/g_{Comp\text{-}B}$) and is close to the value calculated from the latent enthalpy of TNT from [12] corrected for the amount of TNT in Comp-B (e.g. 98 $J/g_{TNT} \times 0.4\ g_{TNT}/g_{comp\text{-}B}$ = 39 $J/g_{Comp\text{-}B}$). The integral of the average heat flow between 127°C (400 K) and 187°C (460 K) is the enthalpy required to dissolve the RDX (-19 $J/g_{Comp\text{-}B}$). This is much less than the enthalpy associated with the RDX melt (e.g. 148.5 $J/g_{RDX} \times 0.6\ g_{TNT}/g_{comp\text{-}B}$ = 89 $J/g_{Comp\text{-}B}$) and is spread out over a larger temperature range.

The latent enthalpy is modeled using the effective capacitance method that is shown in Figure 2.D and E. A trapezoidal integration of the overall energy flow is separated into latent and caloric contributions to determine the effective heat capacitance as the TNT component in Comp-B melts between 77°C (350 K) and 127°C (400 K) and dissolves the RDX suspension between 127°C (400 K) and 187°C (460 K).The baseline specific heat was determined from [5] using a weighted average of the specific heat of TNT and RDX, $C_p = 2.1538 \times T + 413.15$, with C_p in J/kg-K and T in K).

SANDIA'S INSTRUMENTED THERMAL IGNITION (SITI) EXPERIMENT

Kaneshige et al. [13] described the SITI experiment which is shown schematically in Figure 3.A. The three-dimensional mesh used to model the SITI experiment is shown in Figure 3.B. The location of the thermocouple junctions and typical measured temperatures in the center of the 2.54 cm diameter by 2.54 cm tall cylinder are shown in Figure 3.C and 3.D, respectively.

The outside temperature of the confining aluminum cylinders is maintained at a controlled set point. Typically, the outside temperature of the aluminum confinement was ramped from room temperature until the set point temperature was reached. The ramp rate was controlled so that each experiment reached the set point temperature in about 10 minutes. The experiment has a pressure tap to monitor the pressure during the experiment. The measured pressure for run #420 is shown in Figure 3.D.

Table 1 gives the set point temperature and ignition time for eight SITI experiments. The average mass of the Comp-B in these eight experiments was 21.97 g. The 2.54 cm (1 inch) wide by 2.54 cm (1 inch) tall pellets have a volume of 12.87 cm^3 giving a pellet density of 1.707 g/cm^3. The average height of the 2.22 cm (0.8725 inch) wide expansion volume was 0.32 cm (0.126 inch) making the total volume of the expansion gaps 2.47 cm^3. The average bulk density of Comp-B occupying the pellet volume and the expansion volume is 1.432 g/cc. This density was chosen as the initial density since this volume will be occupied by Comp-B once it melts and thermally expands.

Table 1. SITI runs with Comp-B

Run #	$T_{set\ point}$, K	1000/T	$t_{ignition}$, min.	Mass, g	V_{pellet}, cm^3	$V_{expansion}$, cm^3	ρ_{pellet}, g/cc	ρ_{bo}, g/cc*	Vented
69	453.5	2.205	22.45	21.98	12.87	2.49	1.708	1.431	N
420	451.4	2.215	36.12	21.97	12.87	2.45	1.707	1.434	N
67	448.4	2.230	46.68	22.00	12.87	2.50	1.709	1.431	N
72	445.4	2.245	92.80	21.95	12.87	2.44	1.705	1.434	N
76	443.5	2.255	153.61	21.95	12.87	2.41	1.705	1.436	N
75	441.4	2.266	201.01	22.03	12.87	2.51	1.712	1.433	N
70	453.5	2.205	198.36	21.95	12.87	2.47	1.705	1.431	Y
71	452.4	2.210	221.78	21.97	12.87	2.50	1.707	1.430	Y
			average:	21.97		2.47	1.707	1.432	

*ρ_{bo} is the mass of the pellet divided by the pellet and expansion volumes.

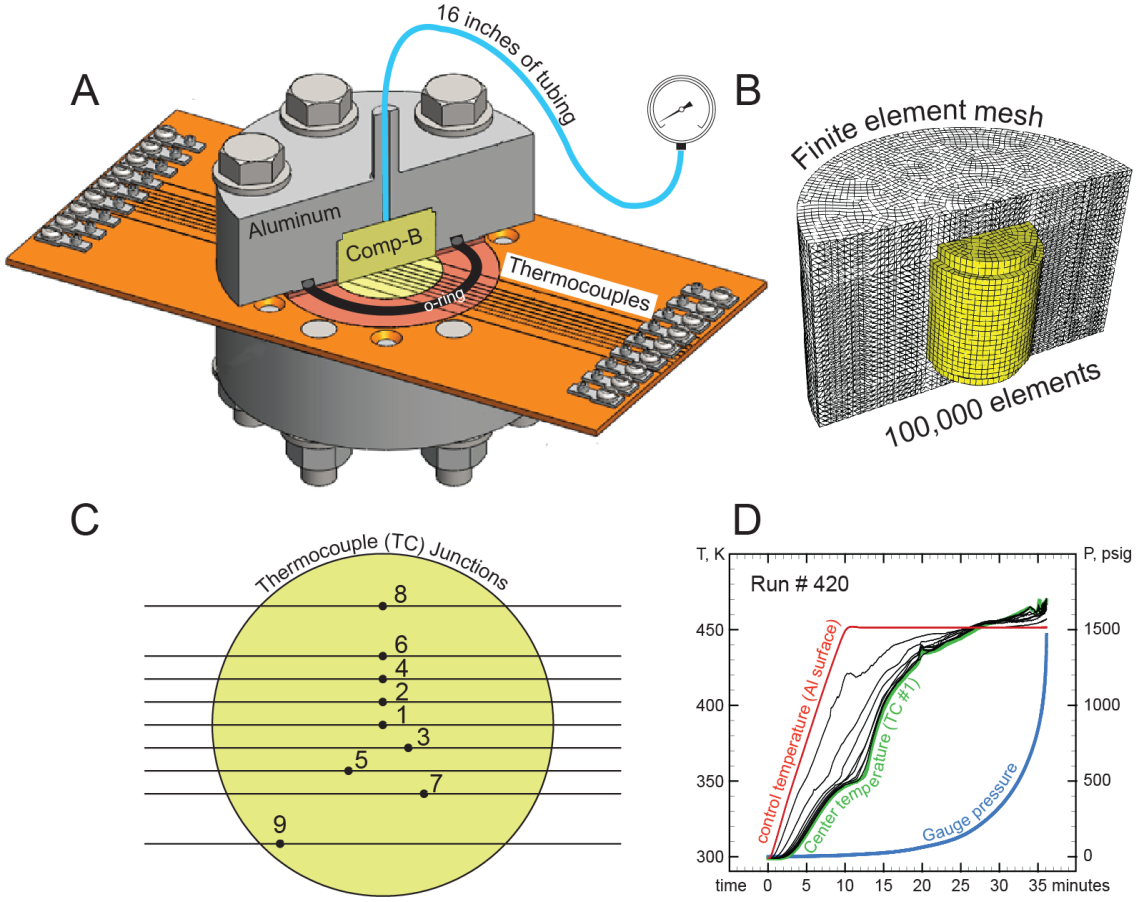

Figure 3 SITI A) schematic B) mesh, C) thermocouple locations, and D) typical measurements.

OVEN TEST

Figures 4.A, 4.B, and 4.C show a schematic of an oven test wherein flaked Comp-B is melted and cooked in a convection oven. Figure 4.D shows the finite element mesh. Two 4 inch (10 cm) diameter by 3 inch (7.6 cm) tall cylinders are shown welded together in Figure 4.E. The bottom cylinder has a notch on the top, where it is welded to the top cylinder that has a similar notch on both the top and the bottom. Both cylinders are filled with flaked Comp-B such that when the Comp-B melts, the bottom cylinder fills with molten Comp-B. Three thermocouple probes are located in the bottom cylinder and are 0.75 inches (1.9 cm) from the center at 90°, 180°, and 270°. The thermocouples are positioned at different axial locations with the top, center, and bottom thermocouple located 1 inch (2.54 cm), 1.5 inches (3.8 cm), and 2 inches (5.1 cm) from the back wall, respectively.

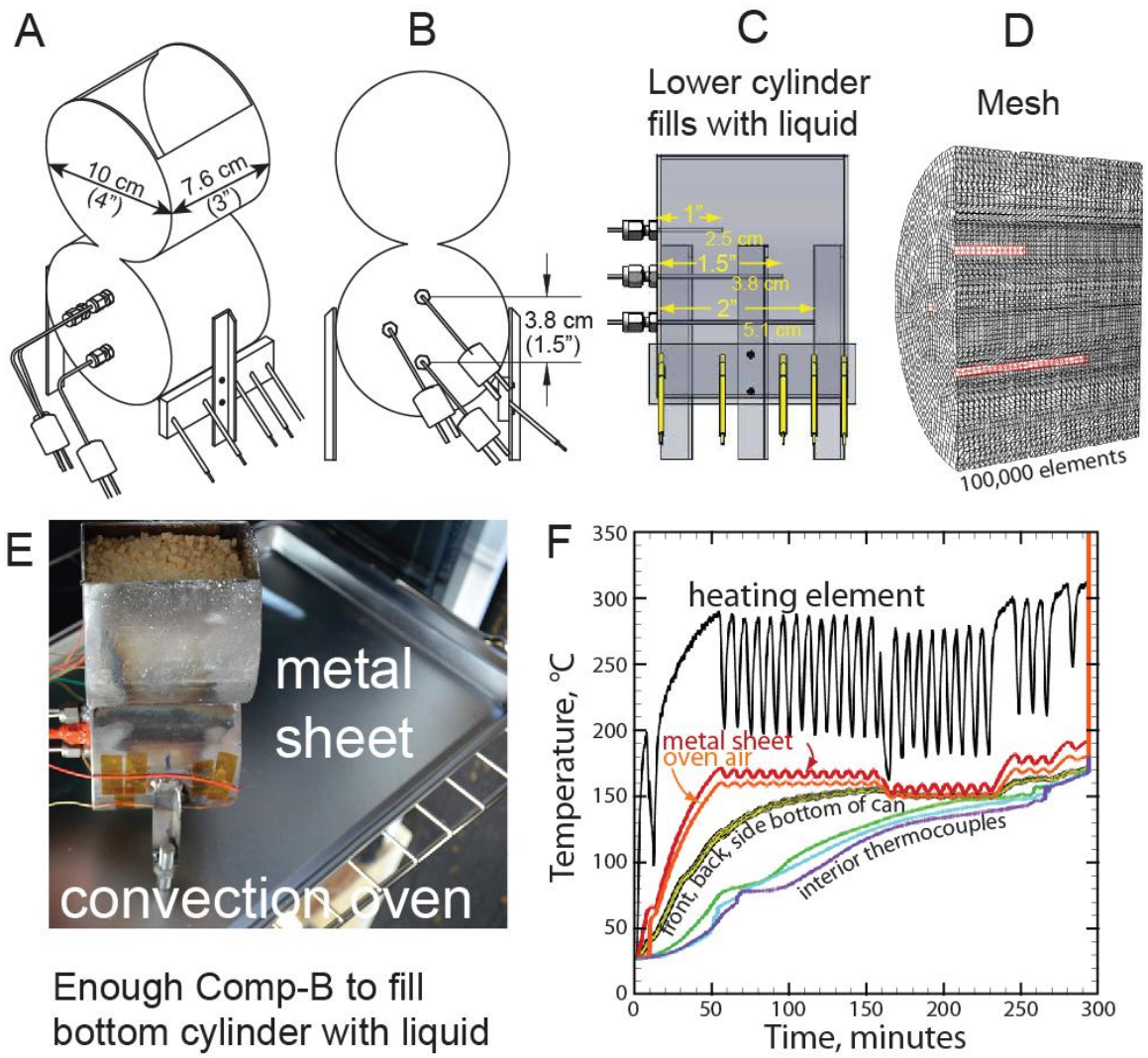

Figure 4 Schematic (A-C), picture (D) and measured temperatures (E) for oven test.

Figure 4.E shows a picture of the oven test. Figure 4.F is a plot of the measured temperatures of the heating element, the metal sheet placed under the test apparatus, and the oven air. The temperature of the front, back and side of the bottom cylinder show a uniform boundary temperature on the bottom cylinder. The interior thermocouples show the melting of the TNT at about 80°C and the subsequent liquefaction of the RDX suspension between 140 and 160°C. When the suspension of RDX particles is melted, the convective cells cause the liquid to mix and the temperatures to pinch together. Eventually, the liquid goes into thermal runaway.

MODEL

The finite element model ARIA [14] was used to solve the one temperature mixture model with a volumetric reaction source as shown in Table 2. All of the wetted surfaces were assumed to have a no-slip boundary condition with the velocity set to zero at these locations. The temperature of the gas and condensed phases are assumed to be the same, that is, $T_c = T_g = T(x,y,z,t)$ and the velocity of the gas phase and condensed phase are also assumed to be equal $V_c = V_g = V(x,y,z,t)$. The model uses a low Mach flow assumption, where the gas velocity is much less than sound speeds and the pressure within the system is only a function of time, that is, $P(x,y,z,t) = P(t)$. The reaction mechanism and auxiliary equations are given in Table 3. Model parameters are given in Table 4.

Table 2. One temperature mixture model for low Mach number flows ($\nabla P \approx 0$).*

Gas pressure (low Mach)	$P_g(x,y,z,t) = P_g(t) = \dfrac{\bar{z}nR\bar{T}}{V_g}$	(1)
Momentum (integral)	$\rho\dfrac{d\vec{v}}{dt} + \rho\vec{v}\cdot\nabla\vec{v} = -\nabla P + \mu\nabla^2\vec{v} + (\rho - \rho_o)gh$	(2)
Energy (field)	$\rho C_p\dfrac{\partial T}{\partial t} + \rho C_p\vec{v}\cdot\nabla T = \nabla\cdot(k\nabla T) + qr$	(3)

* C_p, k, Λ, μ, P, P_g, q, r, ρ, R, t, T, $\bar{T}$, V, V_g, $\vec{v}$, x, y, z, and $\bar{z}$ represent the bulk specific heat, thermal conductivity, region containing Comp-B, bulk viscosity, mixture pressure, gas pressure, reaction enthalpy, reaction rate, bulk density, gas constant, time, temperature, average temperature, volume, gas volume, bulk velocity, x-coordinate, y-coordinate, z-coordinate, and gas compressibility, respectively.

Table 3. Reaction mechanism and auxiliary equations*

Mechanism†	Comp-B ($C_{4.58}H_{5.61}N_{4.82}O_6$) $\rightarrow 2.41N_2 + 2.24H_2O + 1.88CO_2 + 0.25CH_4 + 0.064H_2 + 2.45C + 5.82\times10^6$ J/kg	(1)
Overall Reaction Rate	$r = A\left(\frac{P}{P^o}\right)^{n_p}\lambda\exp\left[-(E+\xi\sigma_E)/RT\right][\text{compb}]$	(2)
Comp-B reaction rate	$r_{CompB} = \frac{d}{dt}[\text{compb}] = -r$	(3)
Gas reaction rate	$r_{gas} = \frac{d}{dt}[\text{gas}] = +6.845r$	(4)
Carbon reaction rate	$r_{carbon} = \frac{d}{dt}[\text{carbon}] = +2.450r$	(5)
Liquid rate multiplier	$\lambda = \delta + (1-\delta)15$, where $\delta = 0.5\left\{1-\tanh\left[\frac{(T-T_d)}{w_d}\right]\right\}$	(6)
Distribution parameter	$\xi = invsnorm(1-[\text{compb}]/[\text{compb}_o])$	(7)
Gas volume fraction	$\phi = 1-\left[S_f\rho_{co}(1-\phi_o)/\rho_c\right]$	(8)
Reacted solid fraction	$S_f = \left([\text{Comp-B}]M_{wCompB} + [\text{carbon}]M_{wcarbom}\right)/\rho_{bo}$	(9)
Initial gas volume fraction	$\phi_o = (\rho_{co}-\rho_{bo})/(\rho_{co}-\rho_{go})$	(10)
Gas volume	$V_g = \int_\Lambda \phi dV$	(11)
Compressibility	$\bar{z} = 1 + X\exp(0.298X)$, where $X = \left(\frac{n}{V_g}\right)\left(\frac{0.0105\times Covol}{\sqrt{\bar{T}+6620}}\right)$	(12)
Moles of gas	$n = \int_\Lambda [gas]dV$	(13)
Average gas temperature	$\bar{T} = \int_\Lambda \rho_b C_p T dV / \int_\Lambda \rho_b C_p dV$	(14)
Condensed density	$\rho_c = \rho_{co}\left[1-\beta(T-T_o)\right]$	(15)
Vol. expansion coefficient	$\beta = \beta_o + \beta_o(\gamma-1)(T-300)/200$	(16)

* A, β, carbon, compb, $compb_o$, Covol, C_p, δ, E, ϕ, ϕ_o, gas, γ, invsnorm, λ, Λ, M_{wCompB}, $M_{wcarbon}$, n, n_p, P, P_o, r, r_{carbon}, r_{compb}, r_{gas}, R, ρ_c, ρ_c^o, ρ_b, ρ_b^o, ρ_{go}, σ_E, T_d, T, T_o, $\bar{T}$, V, V_g, X, $\bar{z}$, ξ represent prefactor, volumetric thermal expansion coefficient, molar composition of carbon, molar composition of Comp-B, initial molar composition of Compb-B, BKWS gas covolume, bulk specific heat, delta function (0 when $T < T_d$, 1 when $T \geq T_d$), activation energy, gas volume fraction, initial gas volume fraction, molar composition of gas, volumetric expansion factor (e.g. multiplier at 500 K), inverse of the standard normal distribution, liquid rate multiplier, region containing Comp-B, moles of gas, pressure exponent, pressure, initial pressure, reaction rate, carbon reaction rate, Comp-B reaction rate, gas reaction rate, gas constant, condensed density, initial condensed density, bulk density, initial bulk density, initial gas density, standard deviation of activation energy, dissolution temperature, temperature, initial temperature, energy averaged gas temperature, volume, gas volume, BKWS parameter, BKWS gas compressibility, distribution parameter, respectively.

†Confined decomposition with prolonged contact of reactive species may justify the assumption that the decomposition products go all the way to final equilibrium products, which is certainly not observed in unconfined experiments [6]. If this assumption is wrong, than other parts of the model must also be wrong to get a good fit to the data. For example, the heat of reaction would be different if the products included N_2O and CH_2O, but the pressurization would also be different.

Table 3. Model Parameters*

Parameter	Description	SITI	Oven Test
β_o	Vol. expansion coefficient [12]	0.0001638	0.0001638
Covol	BKWS covolume, Å^3	475	475
C_p, J/kgK	Bulk specific heat	Figure 2.D	Figure 2.D
E/R, K	Activation Energy/R	22000	22000
ϕ_o	Initial gas volume fraction	0.18	0.03
γ	Expansion multiplier at 500 K	10	10
k, W/mK	Thermal conductivity (T< 353 K)	0.17	0.17
k, W/mK	Thermal conductivity (T> 355 K)	0.12	0.12
k, W/mK	Thermal conductivity (353 ≤ T ≤ 355)	linear interpolate	linear interpolate
λ_m	Liquid rate multiplier	15	15
Ln *A*, Ln (1/s)	Natural logarithm of A	35.67	35.67
μ, Pa·s	Viscosity (T< 412.5 K)	0.25×10^6	0.25×10^6
μ, Pa·s	Viscosity (T> 413.5 K)	0.2	0.2
μ, Pa·s	Viscosity (412.5 K ≤ T ≤ 413.5 K)	linear interpolate	linear interpolate
M_{wcompb}, g/mol	Molecular weight of Comp-B	224.1	224.1
M_{wg}, g/mol	Average gas molecular weight	28.4	28.4
M^o_{wg}, g/mol	Initial gas molecular weight (air)	28.0	28.0
P_o, bars (psi)	Initial pressure	0.83 (12.09)	0.83 (12.09)
n_p	Pressure exponent	0 (vented) 0.725 (confined)	0 (vented)
q, J/kg	Reaction enthalpy	5.82×10^6	5.82×10^6
ρ_b^o, kg/m^3	Initial bulk density	1432	1700
ρ_c^o, kg/m^3	Initial condensed density	1750	1750
ρ_g^o, kg/m^3	Initial gas density	0.944	0.944
σ_E / R, K	Distribution parameter	-500	-500
T_d °C	Dissolution point	453.7	453.7
V_{enc}, cm^3	Enclosure volume	0.56-0.64	0.56-0.64
V_{rdx}, cm^3	Bulk RDX volume	12.9	12.9
V_{tube}, cm^3	Pressure tubing volume	0.84	0
w_d °C	Dissolution temperature width	5	5

* The bulk specific heat includes an effective capacitance model as shown in Figure 2.D. The effective capacitance model is used for the latent phase change of TNT and the dissolution of RDX. The thermal conductivity changes at the melting point of TNT. The viscosity changes from a solid like material to a liquid as the RDX suspension begins to dissolve.

The bulk densities in Table 3 for both the SITI and oven test are not the starting bulk density in either experiment. The average initial bulk density in the SITI experiment is the density of the pellets, ρ_{pellet} = 1701 kg/m^3, as given earlier in Table 1. In Table 3, the bulk density was taken to be the mass of Comp-B divided by the volume that the pellet plus the ullage volume. The ullage volume allows for thermal expansion of the Comp-B. In the oven test, the actual initial bulk density is half of what is listed in Table 3, since two volumes are initially filled with Comp-B flakes. As the Comp-B melts and thermally expands, the lower cylinder is filled with all of the material giving the density as given in Table 3. Since the melt, flow, and filling of the lower cylinder is beyond the scope of the current analysis, the initial bulk density was taken to be the measured mass of Comp-B divided by the volume of the lower cylinder, as given in Table 3. The thermal conductivity was fit to match measure temperature profiles and may be higher than given in Table 3 because of the assumption regarding the initial density. Future work should address the discrepancy in the assumed bulk densities and the actual bulk densities.

Not all of the required properties are known for Comp-B, especially at elevated temperatures. For example, the viscosity as a function of temperature is not known over the entire temperature range of the experiments. In reference [1], the viscosity of Comp-B is given as 0.31 at 83°C and 0.27 at 90°C. Nunez et al. [15] found the viscosity of Comp-B to be shear thinning with the viscosity being 0.2 at 135°C. The viscosity is complex in that it changes with the extent of reaction. In the current work, we assume that the viscosity changes from a solid-like material to a liquid with a viscosity of 0.2 at 140°C, which is the temperature where the RDX suspension begins to dissolve in the hot TNT.

Both the pressure dependent reactions and the swelling characteristics of the Comp-B are not known. This leads to model parameters that are confounded. In other words, the pressure dependency is correlated with the available gas volume, which depends on the unknown expansion properties of Comp-B. The volumetric expansion coefficient given in Table 1 was only given at room temperature. This coefficient is assumed to be temperature dependent, similar to the volumetric expansion coefficient for RDX [7]. The temperature dependency given in equation (16) in Table 3 was chosen to give a linear temperature dependency with gamma representing the thermal expansion multiplier at 500 K. For example, β is 10 times higher at 500 K than at 300 K when γ is 10. If the swelling model is wrong, then the pressure dependency is also wrong. With more data, the swelling and pressure dependency should be reevaluated.

RESULTS

This section compares predicted and measured temperatures, pressures, and ignition times for the SITI experiments. As a validation, predictions of the temperature in the oven test are also compared with data.

SITI COMPARISONS

Figure 5.A shows the measured and predicted time-to-ignition for the eight SITI experiments listed in Table 1. The ignition plot is annotated with the run number next to each of the data symbols. The solid symbols represent runs that were sealed and the open symbols represent runs that are vented. For the vented experiments, the pressure exponent, n_p, was set to zero. For the sealed experiments, pressure exponent was 0.725 as given in Table 3.

Figures 5-B through 5.I show the measured and predicted temperatures and pressures for the eight SITI experiments. The location of the nine of the ten temperatures shown in Figure 5 are shown in Figure 3.C. The hottest temperature is the control temperature, which is located on the exterior of the SITI apparatus. Experiments #70 and #71 did not have pressure measurements since these were vented experiments. The pressure measurement was missing from experiment #72, which was a sealed experiment. In Experiment #66 the pressure tubing

plugged. Also in experiments #75 and #76, the pressure transducer did not record pressures greater than 5000 psig (345 bars).

The predicted time-to-ignition for the sealed experiments match the measured ignition times adequately. However, the vented experiment #71 ignited faster than predicted. If the vent hole clogged in experiment #71, the measured ignition time would have been faster than the prediction, since the reactions are pressure dependent. Future work should include more vented experiments for a better statistical representation of venting effects.

The measured temperatures are adequately described by the model up until about 430 K. At 430 K, the model predicts that all of the Comp-B is melted and convective heat transfer causes the ten internal temperatures to come together. This temperature equilibrium is not as rapid in the experiments implying that the change in viscosity is not as rapid as assumed in the model.

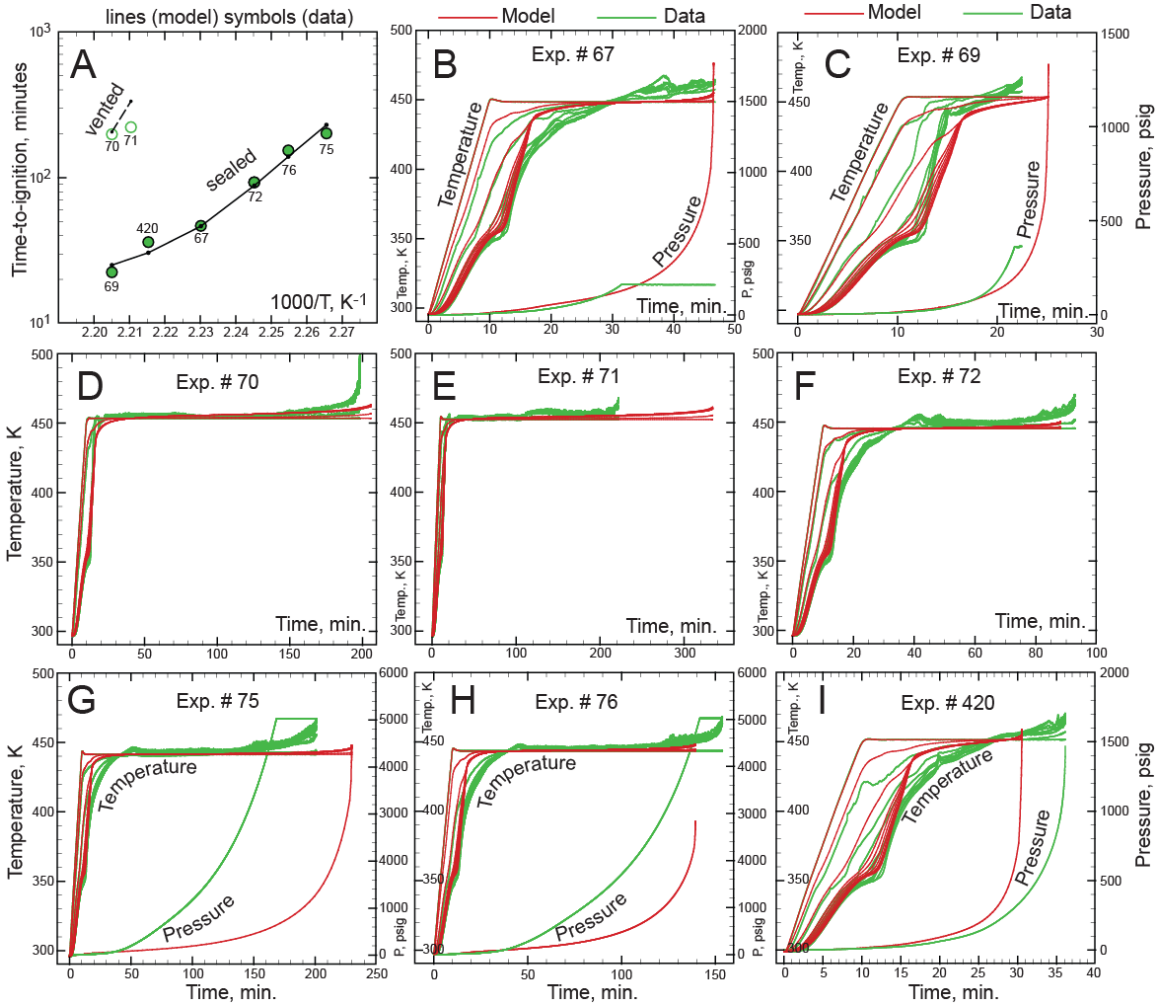

Figure 5. Predicted and measured time-to-ignition, temperature, and pressure for the eight SITI experiments listed in Table 1. The location of the 9 internal temperatures is shown in Figure 3.A. The hottest temperature is the control temperature located on the exterior of the SITI apparatus.

OVEN TEST COMPARISONS

Figure 6 shows several center slices of the oven test at various times. The temperature scale is adjusted so that the minimum temperature is blue and the maximum temperature is red. The minimum and maximum temperatures are shown at the bottom of the cut plane on each image. The minimum and maximum Comp-B velocity is also shown on each image.

In Figure 6, the outer confining can is shown as a transparent grey. The solid Comp-B is shown as a transparent surface within the transparent grey confining cylinder. At 50 minutes all of the Comp-B is solid and thus, no inner transparent surface is shown. At 100 minutes, the outer edges are liquid and there is a large solid plug shown as a transparent orange surface at 100 minutes. The solid Comp-B is shown as a transparent yellow surface at 150 minutes and a greenish-blue transparent surface at times greater than 150 minutes.

The RDX in the Comp-B initially melts near the outer confining shell and moves toward the center of the bottom thermocouple. The solid plug eventually gets smaller and starts to fall toward the bottom of the can, before it completely melts. The maximum velocity occurs as the final solid plug of Comp-B settles to the bottom of the apparatus and eventually melts. After the Comp-B is completely melted, the liquid heats up and eventually self-heats, and ignites at the top of the can.

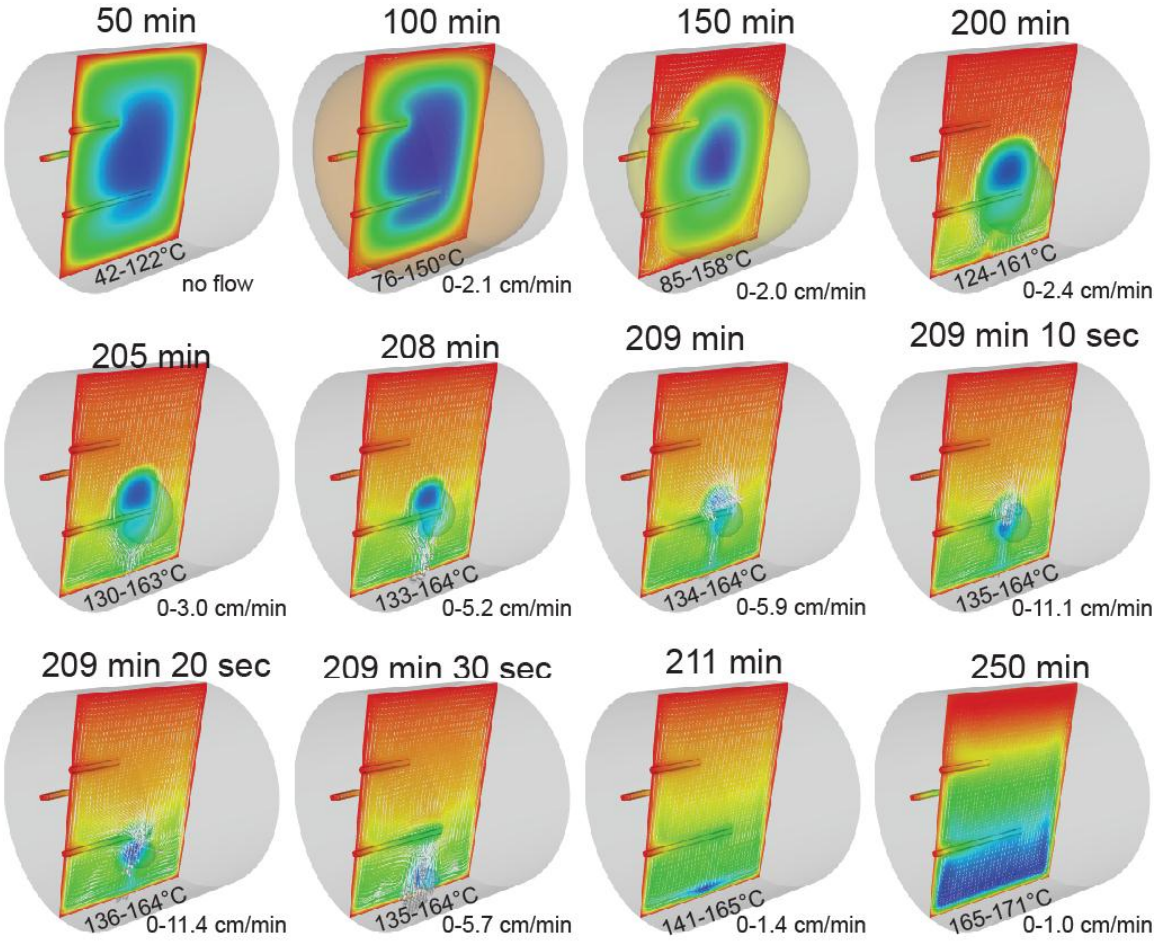

Figure 6. Predicted temperatures and velocities of Comp-B heated in a convective oven. The outer boundary temperature was specified using the average thermocouple measurements of the front, back, and side of the confining can as given in Figure 4.F. The outer transparent gray surface is the confining vessel and the inner transparent surface defines the solid Comp-B. The temperatures listed in each plot represent the minimum (blue) and maximum (red) predicted temperatures.

Figure 7 shows the top, middle, and bottom probe temperatures. The approximate range of the TNT melt and RDX dissolution are also shown in Figure 7. These ranges are based on the DSC data shown previously in Figure 2.B. The six color plots in Figure 7 show the temperature at a center cut plane through the experimental apparatus. The black line in the color plots at 100, 150, and 200 minutes is the 140°C isotherm which defines where the viscosity changes from a high value (2.5×10^5 Pa·s) to a low value (0.2 Pa·s). The predicted ignition point is at approximately 330 minutes and the measured ignition point is at 280 minutes. The discrepancy in the ignition time could be related to the method of melting the Comp-B flakes. In the experiment, the flakes were melted in the combined system as shown in the picture in Figure 4.E. In the model, the total mass of the flakes were assumed to be located in the bottom cylinder. The agreement between the model and experiment is adequate.

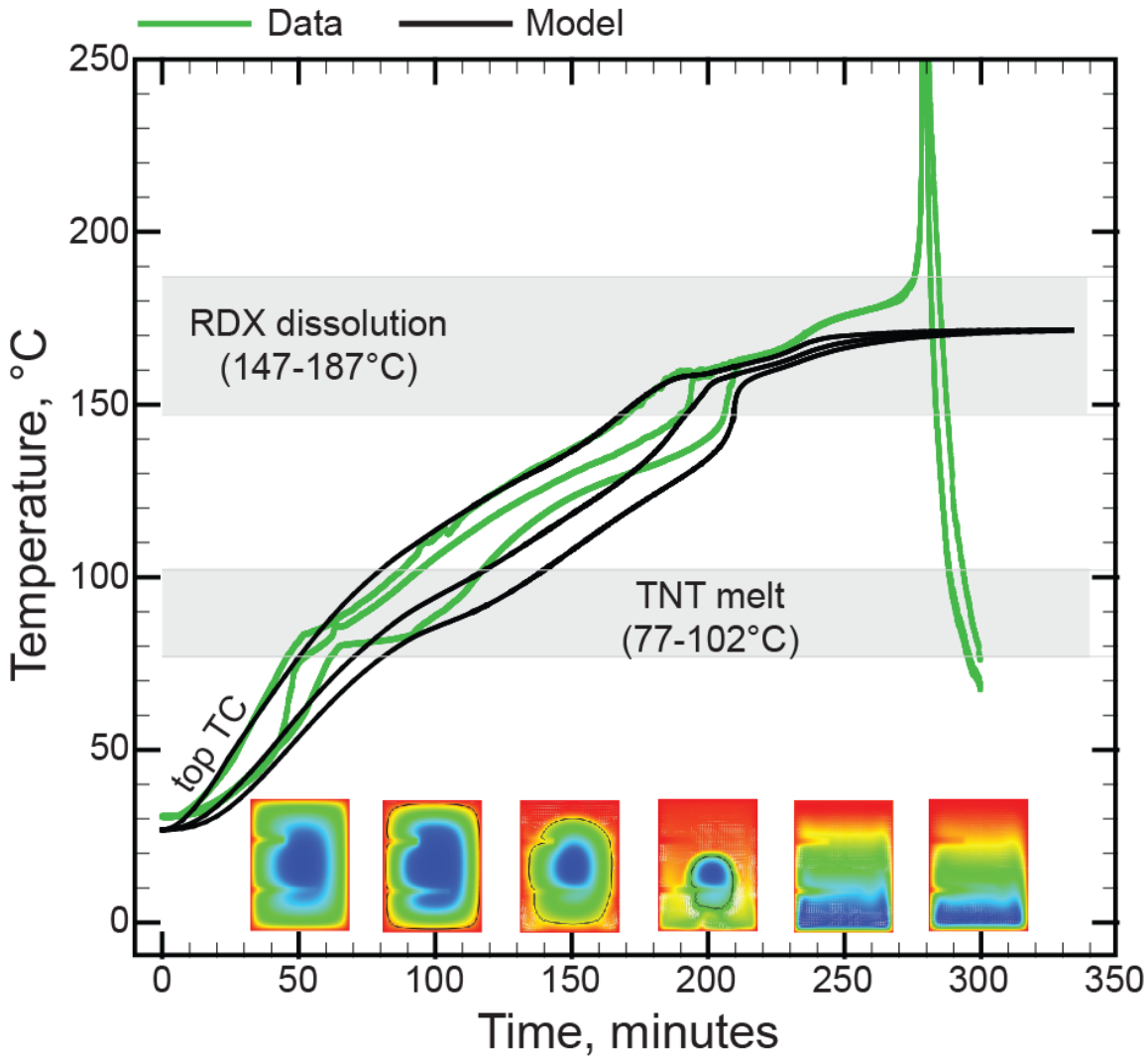

Figure 7. Measured and predicted internal temperature in the oven test. The color plots are the temperature of a slice through the center of the test apparatus. Blue corresponds to the coldest temperature and red corresponds to the hottest temperature. The black lines on the color plots at 100, 150, and 200 minutes define the boundary of the liquid Comp-B and the solid Comp-B.

SUMMARY AND CONCLUSIONS

Decomposition of Comp-B is different than decomposition of the individual constituents that comprise Comp-B: TNT and RDX. In Comp-B, TNT melts at the same temperature as in pristine TNT; however, the RDX does not melt at the same temperature as pristine RDX. In fact, the hot TNT seems to dissolve the RDX at lower temperatures than the RDX melting point. As Comp-B is heated, the TNT melts and leaves the RDX in suspension. Eventually, the suspension begins to dissolve and the liquid starts to move as convection starts to become significant. Eventually, the hot liquid generates more energy than can be dissipated by conduction and convection, leading to thermal runaway. The predicted location of ignition was primarily at the top of the experiment as the hot, less-dense liquid moved to the top of the confining apparatus.

Cookoff of Comp-B is a four-phase reactive flow problem. The four phases are the solid Comp-B, the liquid TNT, the RDX in suspension, and the decomposition gases. In the current work, cookoff of Comp-B was modeled as a one-phase reactive flow problem wherein the solid, liquid, and gas were assumed to be at the same local temperature and velocity. All of the simulations were made using a three-dimensional finite element code using multiple processors solving one energy equation, one momentum equation, and three continuity equations. A single-step, pressure-dependent, distributed activation energy model was used to model the decomposition of Comp-B. The model also assumes that the rate increases by a factor of 15 once the RDX is dissolved. The decomposition product hierarchy is based on the equilibrium composition. The pressure is calculated using a low Mach flow assumption in conjunction with the BKWS-EOS. The kinetic parameters were obtained by matching data from the SITI experiment and the model was validated with a larger scale oven test.

The model and the data were in fair agreement. However, some simplifying assumptions may have led to divergence between the model and data. For example, the initial density in the oven experiment was assumed to be the total mass of Comp-B divided by a confining volume. However, in the experiment, flaked Comp-B was melted in situ until the containing volume was filled with the Comp-B melt. This complexity was beyond the current modeling capability. However, the simplified assumption did provide insight into the decomposition and eventual cookoff of unconfined Comp-B. Noteworthy simulations of the SITI experiment included both vented and sealed experiments. The vented and sealed experiments were used to determine the effect of pressure on the reaction rates of Comp-B.

ACKNOWLEDGMENTS

We would like to thank Craig Tarver and Tri Tran at Lawrence Livermore National Laboratory (LLNL) for supplying the ODTX data for Comp-B, Tom Massis at Sandia National Laboratories (SNL) for supplying the pure TNT for the TGA/DSC samples, Bob Patton (SNL) for running the TGA/DSC experiments, Shane Snedigar (SNL) for running the SITI experiments, Dave Zerkle at Los Alamos National Laboratory (LANL) for many discussions regarding cookoff and viscosity of Comp-B, Mel Baer (SNL) for discussions regarding decomposition of melt-castable explosives, Bill Erikson (SNL) and Steven Todd (SNL) for internal review, and Clint Hall, Anthony Geller, Leanna Minier for management support.

REFERENCES

1. Fedoroff, B. T., Sheffield, O. E., ***Encyclopedia of Explosives and Related Items***, PATR 2700, Volume 3, U. S. Army Research and Development Command, Picatinny Arsenal, New Jersey, USA (1966).
2. Singh, S., Jelinek, L., Samuels, P., Di Stasio, A., Zunino, L., "IMX-104 Characterization for DoD Qualification," *2010 Insensitive Munitions & Energetic Materials Technology Symposium*, Munich, Germany (2010).
3. Fung, V., Ervin M., Alexander, B., Patel, C, Samuels, P., "Development and manufacture of an Insensitive Composition B Replacement Explosive IMX-104 for Mortar Applications," *2010 Insensitive Munitions & Energetic Materials Technology Symposium*, Munich, Germany (2010).
4. Zerkle, D. K., "Composition B Decomposition and Ignition Model," *Thirteenth International Detonation Symposium,* ONR 351-07-01, Office of Naval Research, Arlington, VA 771 (2006).
5. McGuire R.R, and Tarver, C.M., "Chemical Decomposition Models for the Thermal Explosion of Confined HMX, TATB, RDX, and TNT Explosives," *Seventh Symposium (International) on Detonation*, NSWC MP 82-334, Naval Surface Weapon Center, White Oak, Silver Spring, MD, 56 (1981).
6. Maharrey, S. and Behrens, R. Jr., "Thermal Decomposition of Energetic Materials. 5. Reaction Processes of 1,3,5-Trinitrohexahydro-s-triazine Below Its Melting Point," *J. Phys. Chem. A.*, **109**, 11236 (2005).
7. Hobbs, M. L., Steyskal, M., Kaneshige, M. J., "Modeling RDX Ignition," *JANNAF 24th Propulsion Systems Hazards Meeting*, Boston, MA (2008).
8. Hobbs, M. L., Kaneshige, M. J., Gilbert, D. W., Marley, S. K., and Todd, S. N., "Modeling TNT Ignition," *J. Phys. Chem. A*, **113**, 10474 (2009).
9. Dobratz, B. M., "LLNL Explosives Handbook—Properties of Chemical explosives and Explosive Stimulants," Lawrence Livermore National Laboratory report, DE85-015961, Livermore, CA (1981).
10. Brill T. B., Gongwer, P. E., and Williams, G. K., "Thermal Decomposition of Energetic Materials. 66. Kinetic Compensation Effects in HMX, RDX, and NTO," *J. Phys. Chem.*, **98**, 12242 (1994).
11. Hobbs, M. L., Baer, M. R., and McGee, B. C., "JCZS: An Intermolecular Potential Database for Performing Accurate Detonation and Expansion Calculations," *Propellants, Explosives, Pyrotechnics*, **24**, 269, (1999).
12. Gibbs, T. R. and Popolato, A., Editors, **LASL Explosive Property Data**, University of California Press, Los Angeles, CA (1980).
13. Kaneshige, M. J., Renlund, A. M., Schmitt, R. G., and Erikson, W. W., "Cook-off Experiments for Model Validation at Sandia National Laboratories," *Twelfth International Detonation Symposium*, ONR 333-05-2, Office of Naval Research, Arlington, VA, 821 (2002).
14. Notz, P. K., Subia, S. R., Hopkins, M. M., Moffat, H. K., and Noble, D. R. *ARIA Manual Aria 1.5: User's Manual*, Sandia National Laboratories Report SAND2007-2734, Albuquerque, NM (2007).
15. Nunez, M. P., Zerkle, D. K., and Zucker, J. M., "The rheology of molten Composition B," Los Alamos Report LA-UR-12-24029, Los Alamos, NM (2012).